

Dual-Polarization GNSS-R for Reflective Surface Characterization

Daniele Oliveira Silva and Felix Antreich

Abstract—This work proposes a Global Navigation Satellite Systems (GNSS) reflectometry (GNSS-R) approach using only the reflected signals received by a dual-polarization antenna that moves along a surface with different electrical properties. In order to estimate the parameters of interest, a maximum likelihood estimator is derived and its performance is evaluated. The results show that the proposed approach can successfully retrieve the electrical information of dielectric materials. In case of materials with high conductivity the performance of the proposed approach is reduced due to the lower identifiability of the applied signal model parameters.

Keywords—GNSS Reflectometry, Remote sensing, Dual-Polarization, Maximum Likelihood Estimator, Reflection coefficient.

I. INTRODUCTION

The use of satellites as a data source for soil studies has a great advantage, since levels of equal or close global coverage, temporal stability, and homogeneous spatial range are almost impossible to achieve with traditional remote sensing techniques [1]. The most widespread studies, which use Global Navigation Satellite Systems reflectometry (GNSS-R) for remote soil sensing, are related to obtaining the moisture content through a configuration called multipath reflectometry (GNSS-MR) [2]. This configuration is based on the simultaneous reception of multiple paths - direct propagation and indirect reflection - which are tracked through a single signal replica, so the main observable involves constructive and destructive interference between two coherent paths. The interference pattern is usually observed through the signal-to-noise ratio (SNR).

This paper presents a new approach for the characterization of reflective surfaces using GNSS-R. We propose to estimate the relative permittivity, ϵ_r , and the electrical conductivity, σ , of the surface using only the reflected GNSS signals. According to [3], the Earth's surface can be characterized by three parameters, namely: magnetic permeability, μ , the electrical permittivity, ϵ , and the electrical conductivity, σ . The magnetic permeability of the Earth's surface can normally be considered equal to the permeability in a vacuum. The relative permittivity (or dielectric constant) represents the measure of interest in the energy storage capacity of a dielectric medium under the effect of a electric field [4]. Zavorotny et al. showed in [5] that the Earth's surface reflectivity at the GPS frequency is sensitive to the dielectric properties of the soil. Electrical

conductivity is a parameter very little explored in GNSS-R, but obtaining its value is very important for agricultural system's management as an extremely relevant indicator in the classification of soil quality [6].

For all GNSS the transmitted signals are right-hand circularly polarized (RHCP). Upon reflection the polarization changes and the signal becomes elliptically polarized, which can be represented by a superposition of a RHCP and a left-hand circularly polarized (LHCP) signal. In many cases the LHCP signal in this superposition is dominant. However, due to the rough surface scattering mechanisms and the soil dielectric constant, there is a non-negligible scattered RHCP signal that can be detected and used to estimate the biogeophysical parameters [7]. The hypothesis that obtaining soil moisture content can be improved when the LHCP and RHCP components of the reflected signal are collected was proposed by [5] and experimentally confirmed in [7]. This is because the ratio of these two signals is sensitive to soil moisture, mitigating the need to estimate nuisance parameters related to the effects of surface roughness [8]. In [9], [10] both polarizations of the reflected signal are used, but the technique used involves constructive/destructive interference between the direct and reflected signals. Techniques using only the reflected signal considering the RHCP and LHCP components have not been studied systematically yet. Therefore, this paper presents a new approach that uses only the reflected GNSS signals received by a dual-polarization antenna (LHCP and RHCP) to characterize the reflective surface through the estimation of its electrical properties.

II. SIGNAL MODEL

A dual-polarization antenna is receiving the reflected GNSS signals and additive noise is introduced by the antenna and the low-noise amplifier (LNA). The signal at the RHCP output and the LHCP output of the antenna after downconversion can be given as

$$x_L(t) = a_L(t)c(t - \tau(t)) + n_L(t) \in \mathbb{C} \quad (1)$$

$$x_R(t) = a_R(t)c(t - \tau(t)) + n_R(t) \in \mathbb{C}, \quad (2)$$

where

$$a_L(t) = \gamma(t)R_l(\epsilon_{ref}(t), \vartheta(t)) \in \mathbb{C} \quad (3)$$

$$a_R(t) = \gamma(t)R_r(\epsilon_{ref}(t), \vartheta(t)) \in \mathbb{C} \quad (4)$$

are the complex amplitudes of the signals received after the reflection of the satellite signal on ground as a function of time t , $\gamma(t) \in \mathbb{C}$ is the complex amplitude of the satellite signal before reflection on ground, $\tau(t)$ is time-delay of the signal, $c(t) \in \mathbb{R}$ is a pseudo random (PR) spreading sequence used by

Daniele Oliveira Silva and Felix Antreich are with the Department of Telecommunications, Aeronautics Institute of Technology (ITA), São José dos Campos, SP, Brazil, e-mail: danielle19954@gmail.com, antreich@ieee.org; This work was partially funded by the National Council for Scientific and Technological Development (CNPq) under grant 132687/2020-8, 409865/2018-4, and 312394/2021-7.

the respective GNSS satellite, and $n_R(t) \in \mathbb{C}$ and $n_L(t) \in \mathbb{C}$ denote the complex noise terms that can be modelled as complex white Gaussian noise. $R_l(\epsilon_{ref}(t), \vartheta(t)) \in \mathbb{C}$ and $R_r(\epsilon_{ref}(t), \vartheta(t)) \in \mathbb{C}$ denote the circular reflection coefficients corresponding to the LHCP and RHCP, respectively, given by

$$R_l(\epsilon_{ref}(t), \vartheta(t)) = \frac{\cos(\vartheta(t)) - \sqrt{\epsilon_{ref}(t) - \sin^2(\vartheta(t))}}{2(\cos(\vartheta(t)) + \sqrt{\epsilon_{ref}(t) - \sin^2(\vartheta(t))})} - \frac{\epsilon_{ref}(t) \cos(\vartheta(t)) - \sqrt{\epsilon_{ref}(t) - \sin^2(\vartheta(t))}}{2(\epsilon_{ref}(t) \cos(\vartheta(t)) + \sqrt{\epsilon_{ref}(t) - \sin^2(\vartheta(t))})} \quad (5)$$

and

$$R_r(\epsilon_{ref}(t), \vartheta(t)) = \frac{\cos(\vartheta(t)) - \sqrt{\epsilon_{ref}(t) - \sin^2(\vartheta(t))}}{2(\cos(\vartheta(t)) + \sqrt{\epsilon_{ref}(t) - \sin^2(\vartheta(t))})} + \frac{\epsilon_{ref}(t) \cos(\vartheta(t)) - \sqrt{\epsilon_{ref}(t) - \sin^2(\vartheta(t))}}{2(\epsilon_{ref}(t) \cos(\vartheta(t)) + \sqrt{\epsilon_{ref}(t) - \sin^2(\vartheta(t))})} \quad (6)$$

where $\vartheta(t)$ is the reflection angle and¹

$$\epsilon_{ref}(t) = \epsilon_r(t) - j \frac{\sigma(t)}{2\pi f_c \epsilon_0} \in \mathbb{C} \quad (7)$$

with the vacuum permittivity $\epsilon_0 = 8.854187817 \times 10^{-12}$ F/m, the relative conductivity $\sigma(t)$, the relative permittivity $\epsilon_r(t)$, and f_c being the carrier frequency of the signal.

The signals $x_R(t)$ and $x_L(t)$ are correlated over a period of time T_d with the replica PR spreading sequence generated at the receiver based on an estimate of the time-delay $\hat{\tau}(t)$. Thus, the signals after correlation, $y_R[k]$ and $y_L[k]$ can be given as

$$y_L[k] = \frac{1}{T_d} \int_{\frac{T_d}{2}(2k-1)}^{\frac{T_d}{2}(2k+1)} a_L(t) c(t-\tau(t)) c(t-\hat{\tau}(t)) dt + \frac{1}{T_d} \int_{\frac{T_d}{2}(2k-1)}^{\frac{T_d}{2}(2k+1)} n_L(t) c(t-\hat{\tau}(t)) dt = \tilde{a}_L[k] + \tilde{n}_L[k] \quad (8)$$

and

$$y_R[k] = \frac{1}{T_d} \int_{\frac{T_d}{2}(2k-1)}^{\frac{T_d}{2}(2k+1)} a_R(t) c(t-\tau(t)) c(t-\hat{\tau}(t)) dt + \frac{1}{T_d} \int_{\frac{T_d}{2}(2k-1)}^{\frac{T_d}{2}(2k+1)} n_R(t) c(t-\hat{\tau}(t)) dt = \tilde{a}_R[k] + \tilde{n}_R[k], \quad (9)$$

where $k = 0, 1, \dots, K-1$. As we are considering two separate receiver chains for the RHCP and LHCP signals with independent amplification we consider

$$E[\tilde{n}_L[k] \tilde{n}_R[k]] = 0. \quad (10)$$

Assuming that $\gamma(t)$ is constant during the correlation of duration T_d and thus it can be given as $\gamma[k]$ for a duration T_d we can further define

$$\begin{bmatrix} y_L[k] \\ y_R[k] \end{bmatrix} = \underbrace{\gamma[k] \varrho[k] g[k]}_{=\mathbf{y}[k]} \underbrace{\begin{bmatrix} R_l(\epsilon_{ref}[k], \vartheta[k]) \\ R_r(\epsilon_{ref}[k], \vartheta[k]) \end{bmatrix}}_{=\mathbf{r}(\epsilon_{ref}[k], \vartheta[k])} + \underbrace{\begin{bmatrix} \tilde{n}_L[k] \\ \tilde{n}_R[k] \end{bmatrix}}_{=\mathbf{n}[k]} \quad (11)$$

where $\varrho[k] \in [0, 1]$ is the correlation loss at period k as $\hat{\tau}(t) \neq \tau(t)$. In case the estimation error of τ is small $\varrho[k] \approx 1$.

Assuming that $\mathbf{r}(\epsilon_{ref}[k], \vartheta[k])$ is constant for K periods and collecting several periods the signal can be written in matrix notation as

$$\mathbf{Y} = \mathbf{r}(\epsilon_{ref}, \vartheta) \boldsymbol{\gamma}^T + \mathbf{N} \quad (12)$$

with

$$\mathbf{Y} = [\mathbf{y}[1] \cdots \mathbf{y}[K]] \in \mathbb{C}^{2 \times K} \quad (13)$$

$$\mathbf{N} = [\mathbf{n}[1] \cdots \mathbf{n}[K]] \in \mathbb{C}^{2 \times K} \quad (14)$$

$$\boldsymbol{\gamma} = [\gamma[1], \dots, \gamma[K]]^T \in \mathbb{C}^{K \times 1}. \quad (15)$$

III. MAXIMUM LIKELIHOOD PARAMETER ESTIMATION

Instead of the real and imaginary part of the complex amplitude $\gamma[k]$ we will consider

$$\gamma[k] = \alpha[k] e^{j\phi[k]} \quad (16)$$

with amplitude $\alpha[k]$ and phase $\phi[k]$. We define the vectors collecting the amplitudes and phases as

$$\boldsymbol{\alpha} = [\alpha[1], \dots, \alpha[K]]^T \quad (17)$$

$$\boldsymbol{\phi} = [\phi[1], \dots, \phi[K]]^T. \quad (18)$$

Also instead of the real and imaginary part of ϵ_{ref} we will consider

$$\epsilon_{ref} = |\epsilon_{ref}| e^{j \arg\{\epsilon_{ref}\}} \quad (19)$$

with the absolute value $|\epsilon_{ref}|$ and the phase $\arg\{\epsilon_{ref}\}$ of ϵ_{ref} . Assuming a random variable \mathbf{Y} with a complex multivariate Gaussian probability density function (pdf) parameterized by the parameter vector

$$\boldsymbol{\theta} = [\boldsymbol{\alpha}^T, \boldsymbol{\phi}^T, |\epsilon_{ref}|, \arg\{\epsilon_{ref}\}, \vartheta, \sigma_n^2]^T \quad (20)$$

we get

$$p_{\mathbf{Y}}(\mathbf{Y}; \boldsymbol{\theta}) = \frac{1}{(\pi \sigma_n^2)^{2K}} \exp\left(-\frac{1}{\sigma_n^2} \|\mathbf{Y} - \mathbf{r}(|\epsilon_{ref}|, \arg\{\epsilon_{ref}\}, \vartheta) \boldsymbol{\gamma}^T\|_F^2\right), \quad (21)$$

where $\|\cdot\|_F^2$ is the Frobenius norm. The likelihood function with respect to the parameter vector $\boldsymbol{\theta}$ can be given as

$$L(\mathbf{Y}; \boldsymbol{\theta}) = p_{\mathbf{Y}}(\mathbf{Y}; \boldsymbol{\theta}). \quad (22)$$

and the maximum likelihood estimator for $\boldsymbol{\theta}$ is

$$\hat{\boldsymbol{\theta}} = \arg \max_{\boldsymbol{\theta}} \{L(\mathbf{Y}; \boldsymbol{\theta})\} = \arg \max_{\boldsymbol{\theta}} \{\log(L(\mathbf{Y}; \boldsymbol{\theta}))\}. \quad (23)$$

The cost function of the estimator can be reformulated as

$$J(\boldsymbol{\theta}) = \log(L(\mathbf{Y}; \boldsymbol{\theta})) = -2K \log(\pi \sigma_n^2) - \frac{1}{\sigma_n^2} \|\mathbf{Y} - \mathbf{r}(|\epsilon_{ref}|, \arg\{\epsilon_{ref}\}, \vartheta) \boldsymbol{\gamma}^T\|_F^2. \quad (24)$$

Differentiating $J(\boldsymbol{\theta})$ with respect to σ_n^2 and equating it to zero we get the estimate

$$\hat{\sigma}_n^2 = \frac{1}{2K} \text{tr}\{(\mathbf{Y} - \mathbf{r}(|\epsilon_{ref}|, \arg\{\epsilon_{ref}\}, \vartheta) \boldsymbol{\gamma}^T) \times (\mathbf{Y} - \mathbf{r}(|\epsilon_{ref}|, \arg\{\epsilon_{ref}\}, \vartheta) \boldsymbol{\gamma}^T)^H\}. \quad (25)$$

Substituting (25) into the cost function we get

$$J(\boldsymbol{\theta}) = -\frac{1}{K} \text{tr}\{(\mathbf{Y} - \mathbf{r}(|\epsilon_{ref}|, \arg\{\epsilon_{ref}\}, \vartheta) \boldsymbol{\gamma}^T) \times (\mathbf{Y} - \mathbf{r}(|\epsilon_{ref}|, \arg\{\epsilon_{ref}\}, \vartheta) \boldsymbol{\gamma}^T)^H\}. \quad (26)$$

Now, differentiating $J(\boldsymbol{\theta})$ with respect to $\boldsymbol{\gamma}^T$ and equating to zero we get the estimate

$$\hat{\boldsymbol{\gamma}}^T = (\mathbf{r}^H(|\epsilon_{ref}|, \arg\{\epsilon_{ref}\}, \vartheta) \mathbf{r}(|\epsilon_{ref}|, \arg\{\epsilon_{ref}\}, \vartheta))^{-1} \times \mathbf{r}^H(|\epsilon_{ref}|, \arg\{\epsilon_{ref}\}, \vartheta) \mathbf{Y}. \quad (27)$$

¹Neglecting polarization losses

Substituting (27) into the cost function (26) and dropping the terms that are not dependent on θ we get

$$J(\theta) = \frac{\mathbf{r}^H(|\epsilon_{ref}|, \arg\{\epsilon_{ref}\}, \vartheta) \hat{\mathbf{R}}_{\mathbf{Y}\mathbf{Y}} \mathbf{r}(|\epsilon_{ref}|, \arg\{\epsilon_{ref}\}, \vartheta)}{\|\mathbf{r}(|\epsilon_{ref}|, \arg\{\epsilon_{ref}\}, \vartheta)\|_2^2} \quad (28)$$

with

$$\hat{\mathbf{R}}_{\mathbf{Y}\mathbf{Y}} = \frac{1}{K} \mathbf{Y}\mathbf{Y}^H. \quad (29)$$

To solve the derived non-linear problem we can employ an iterative approach based on the space-alternating generalized expectation-maximization (SAGE) algorithm [11], [12]. Hence, we need to solve sequentially and iteratively the following one-dimensional problems

$$\hat{\vartheta} = \arg \max_{\vartheta} \left\{ \frac{\mathbf{r}^H(|\hat{\epsilon}_{ref}|, \arg\{\hat{\epsilon}_{ref}\}, \vartheta) \hat{\mathbf{R}}_{\mathbf{Y}\mathbf{Y}} \mathbf{r}(|\hat{\epsilon}_{ref}|, \arg\{\hat{\epsilon}_{ref}\}, \vartheta)}{\|\mathbf{r}(|\hat{\epsilon}_{ref}|, \arg\{\hat{\epsilon}_{ref}\}, \vartheta)\|_2^2} \right\}, \quad (30)$$

$$|\hat{\epsilon}_{ref}| = \arg \max_{|\epsilon_{ref}|} \left\{ \frac{\mathbf{r}^H(|\epsilon_{ref}|, \arg\{\hat{\epsilon}_{ref}\}, \hat{\vartheta}) \hat{\mathbf{R}}_{\mathbf{Y}\mathbf{Y}} \mathbf{r}(|\epsilon_{ref}|, \arg\{\hat{\epsilon}_{ref}\}, \hat{\vartheta})}{\|\mathbf{r}(|\epsilon_{ref}|, \arg\{\hat{\epsilon}_{ref}\}, \hat{\vartheta})\|_2^2} \right\}, \quad (31)$$

$$\arg\{\hat{\epsilon}_{ref}\} = \arg \max_{\arg\{\epsilon_{ref}\}} \left\{ \frac{\mathbf{r}^H(|\hat{\epsilon}_{ref}|, \arg\{\epsilon_{ref}\}, \hat{\vartheta}) \hat{\mathbf{R}}_{\mathbf{Y}\mathbf{Y}} \mathbf{r}(|\hat{\epsilon}_{ref}|, \arg\{\epsilon_{ref}\}, \hat{\vartheta})}{\|\mathbf{r}(|\hat{\epsilon}_{ref}|, \arg\{\epsilon_{ref}\}, \hat{\vartheta})\|_2^2} \right\}. \quad (32)$$

IV. RESULTS

Several simulations were performed to assess the performance of the proposed maximum likelihood estimator under various conditions. We considered a signal-to-noise ratio (SNR) of 15 dB for $\mathbf{y}[k]$ and an observation interval of the signal of KT_d with $K = 500$. We assumed that the variation in the angle of reflection is insignificant during the observation interval and thus $\mathbf{r}(\epsilon_{ref}[k], \vartheta[k])$ can also be considered constant. Furthermore, we observed that with initialization of ϑ far from the global maximum, the estimator could not converge, therefore, the initialization of ϑ was performed using the positioning estimate based on the received satellite signals. Thus, a good convergence of the algorithm for the parameters necessary to characterize the reflecting surface (parameters of interest), namely $|\epsilon_{ref}|$ and $\arg\{\epsilon_{ref}\}$, could be achieved.

Fig. 1 shows the simulation scenario considered in this work. The dashed line represents the trajectory of the receiving antenna on the reflective surface. The receiving antenna was simulated moving along a square area of 100 m² collecting the signals at $p = 1, \dots, 144$ points along the surface. This reflective surface was simulated for two cases, on the one hand considering a homogeneous composition, i.e., $\epsilon_{ref1} = \epsilon_{ref2}$, and on the other hand considering two different surface characteristics, i.e., $\epsilon_{ref1} \neq \epsilon_{ref2}$.

Fig. 2 presents the expectation of the estimates of the parameters $|\epsilon_{ref}|$ and $\arg\{\epsilon_{ref}\}$ for a homogeneous surface whose composition is a medium dry ground. The graphs in the first column of Fig. 2 present the scenario with the true values of the parameters to be estimated. The first and second row of graphs refer to the parameters $|\epsilon_{ref}|$ and $\arg\{\epsilon_{ref}\}$, respectively, whose actual values are 7.0369 and -0.1024 in radian, respectively. In the first column, showing the true values of the reflective surface, the blue points correspond to the reflection points referring to the satellite with pseudo-random

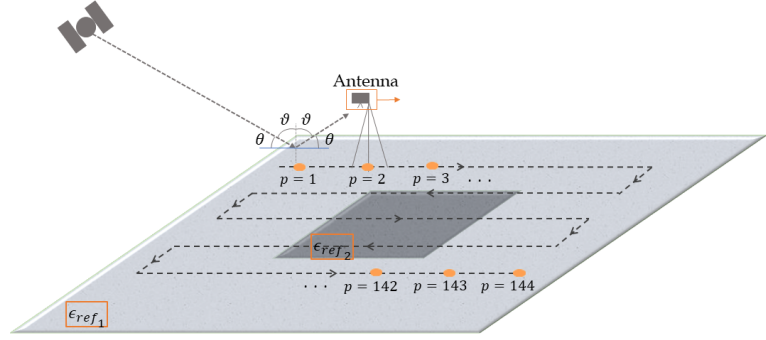


Fig. 1. Simulation scenario.

noise code (PRN) 14 calculated according to the Forward Scatter Geometry [13] and the orange points correspond to the reflection points referring to the satellite with PRN 24. We can observe that the estimator is capable of estimating the surface characteristics quite well in case the elevation angle of the satellite θ is not too high (PRN 24, $\theta > 60^\circ$) which means that the angle of reflection ϑ is small, since ϑ and θ are complementary angles ($\vartheta = \pi/2 - \theta$) according to the Forward Scatter Geometry [13]. The results for the satellite with PRN 24 suggest that the estimator for $|\epsilon_{ref}|$ and $\arg\{\epsilon_{ref}\}$ becomes biased for large θ and thus small ϑ , i.e., the identifiability of the model parameters $|\epsilon_{ref}|$ and $\arg\{\epsilon_{ref}\}$ is reduced for large θ and thus small ϑ .

This performance characteristic of the estimator with respect to ϑ and/or θ can also be observed for all other materials, but for different values of ϑ and θ . Based on the analysis of the estimator's performance and an analysis of the respective cost functions, one can identify a range of ϑ and θ for which the proposed estimator presents good results. For concrete, e.g., according to the simulations performed, it presents good results around $\vartheta = 70^\circ$ presenting a root mean square error (RMSE) of $|\hat{\epsilon}_{ref}|$, $\text{RMSE } |\hat{\epsilon}_{ref}| = 0.14$, where the true value is $|\epsilon_{ref}| = 3$. For fresh water the $\text{RMSE } |\hat{\epsilon}_{ref}| \approx 2.5$, where the real value is $|\epsilon_{ref}| = 80$. Fig. 3 shows for each material the range of ϑ for which the RMSE of $|\hat{\epsilon}_{ref}|$ tends to be small.

On the other hand, the $\text{RMSE } \arg\{\hat{\epsilon}_{ref}\}$ shows that the estimator does not perform well for estimating these parameters when the materials with very low conductivity are used. Concrete, dry ground as well as fresh water are materials with very low conductivity σ compared to the relative permittivity ϵ_r . For these materials the $|\epsilon_{ref}|$ is practically equal to ϵ_r , therefore, σ for these materials is not a significant parameter in the estimation of ϵ_{ref} , since the estimator had a good performance in estimating $|\epsilon_{ref}|$. For other materials analyzed, such as sea water and wet ground, the estimator showed satisfactory results both for $|\epsilon_{ref}|$ and $\arg\{\epsilon_{ref}\}$, because value of σ is larger compared to the value of ϵ_r .

The behavior of the respective cost functions justifies our results, since the larger the curvature of the cost function, the larger the estimation error variance of the algorithm is. In Fig. 4 we show the cost functions considering $\vartheta = 78^\circ$ ($\theta = 12^\circ$) generated for wet ground ($\sigma = 2 \times 10^{-1} S/m$) and for a metallic object ($\sigma = 3.23 \times 10^5 S/m$). For a reflection angle $\vartheta = 12^\circ$ ($\theta = 78^\circ$), the cost functions for the considered

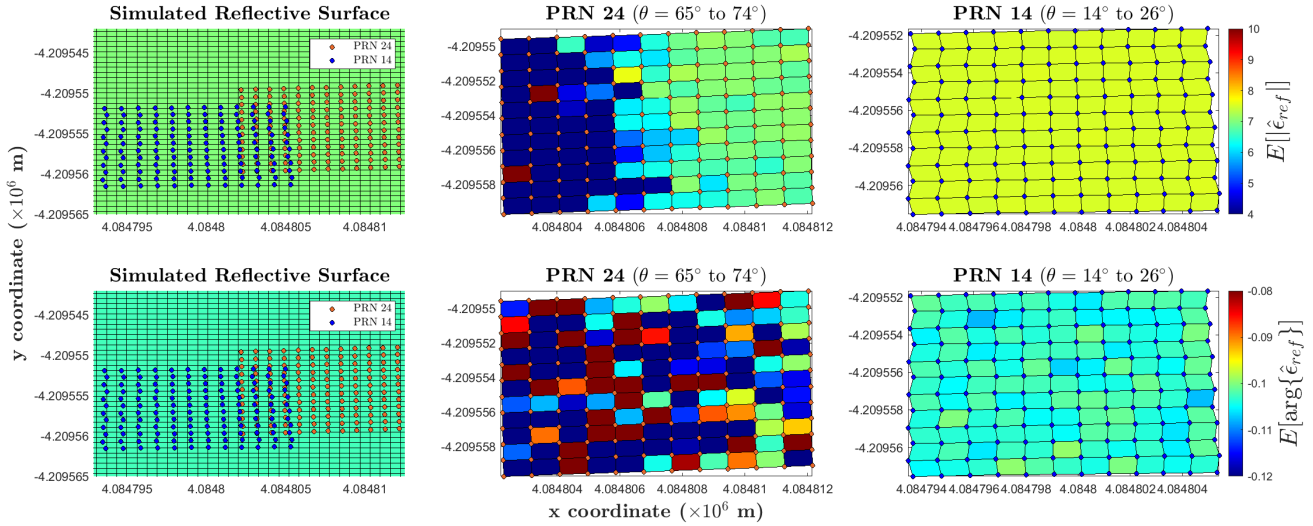


Fig. 2. Estimation result for a reflective surface composed of medium dry ground.

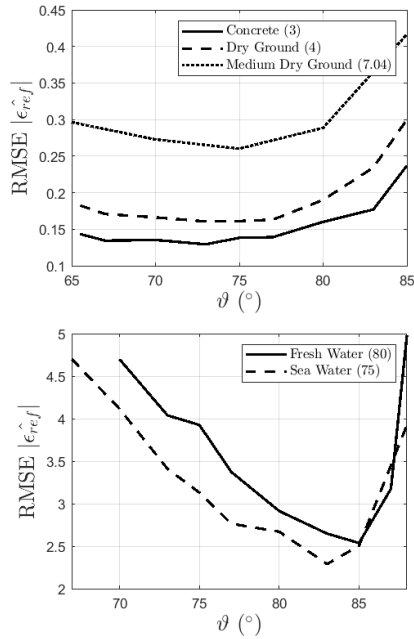


Fig. 3. Behavior of the RMSE $|\hat{\epsilon}_{ref}|$ for high values of ϑ . In the legends the numbers in parentheses are the actual values of $|\epsilon_{ref}|$.

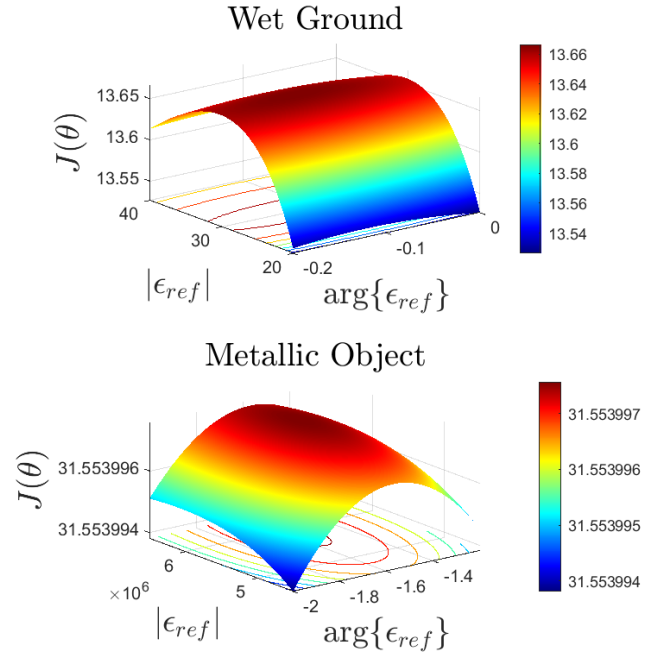


Fig. 4. Cost function analysis for materials with low and high conductivity.

materials vary in the sixth decimal, that is, they present an imperceptible curvature, especially, taking into account a noisy scenario. This behavior can also be observed for materials with very high conductivity σ , i.e., metal surfaces. The cost functions for metallic materials only vary in the sixth decimal as well, even for a reflection angle $\vartheta = 78^\circ$ ($\theta = 12^\circ$). Hence, even considering a low elevation angle, the estimator was not capable to estimate the parameters with high accuracy when metallic materials are considered. Although it is not possible to estimate the parameters of a metallic material with high accuracy (low estimation error variance), it is possible to detect metals when they are present in a dielectric medium. The estimator is provide means for the detection of the

variation in the reflective surface composition, both when this composition has quite different parameters like a metal object on medium dry ground, as well as when this composition varies between materials with similar parameters such as a medium dry ground and wet ground. The results are shown in Fig. 5. The first row of graphs in Fig. 5 shows a surface whose composition is a medium dry ground, represented in blue color, together with a metallic object in red color. In the second row, a surface composed of medium dry ground in blue, together with wet ground represented in red is shown. The points in orange correspond to the reflection points referring to the satellite using PRN 10 and the points in green correspond to the points of reflection referring to the satellite using PRN

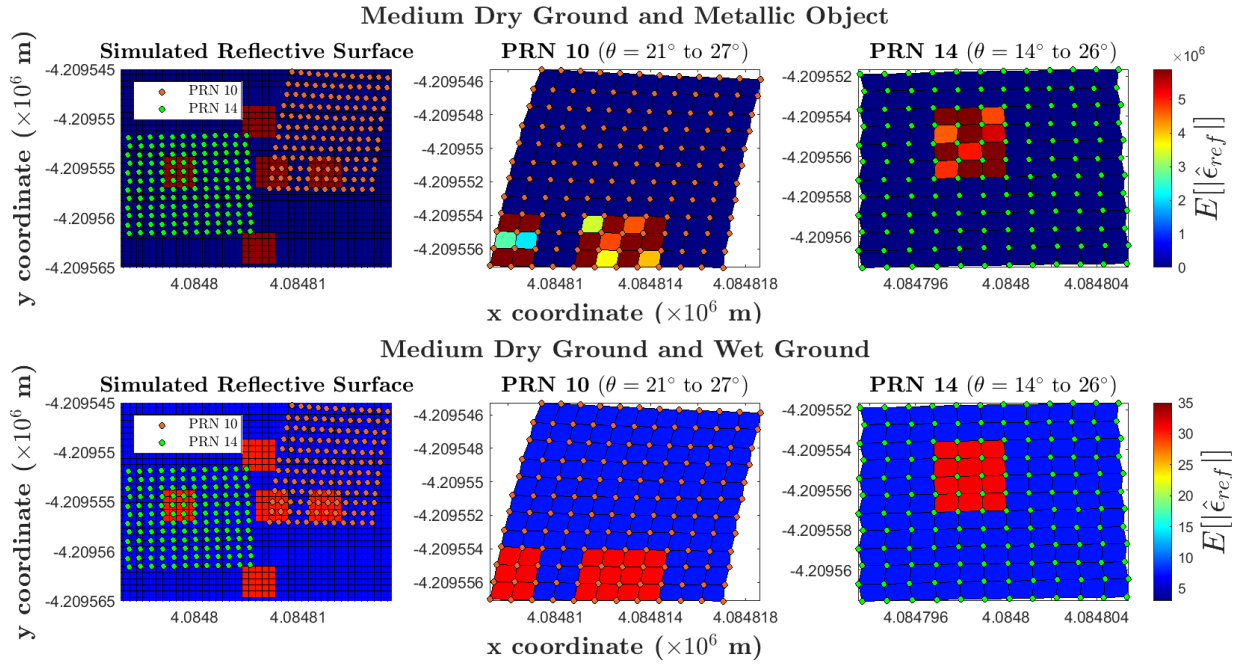


Fig. 5. Performance of the estimator in detecting composition variation on a non-homogeneous reflecting surface.

14.

V. CONCLUSION

We have proposed a new approach to estimate electric properties of a reflective surface based on GNSS-R using only the reflected signals received by a dual-polarization antenna.

The results presented in this work show that a good performance of the proposed estimator is dependent on several parameters, such as the SNR of the received reflected signals, the elevation angle (reflection angle), and the electrical properties of the reflective surface. These properties, that are related to the used parameterization of the received signal and specifically of the reflection coefficients have not been discussed in the literature before, although such parameterizations were applied in several works. Especially, the estimation of the electrical conductivity of reflective surfaces with very low or very high conductivity was assessed in this work.

We conclude that considering the proposed signal model, it is possible to achieve good estimates of the electrical properties of the reflective surface in case it is composed of dielectric materials. For the estimation of electrical properties considering a reflective surface composed of metals or metallic objects, further studies need to be carried out. Despite this, our results show that the detection of metals and metallic objects located on a dielectric media could be achieved well based on the results of the proposed estimator. In addition, our estimator is also capable of providing results that can be used for detecting rather small variations of the composition of the reflective surface.

REFERENCES

- [1] K. Yu, C. Rizos, D. Burrage, A. G. Dempster, K. Zhang, and M. Markgraf, "An overview of gnss remote sensing," *EURASIP Journal on Advances in Signal Processing*, vol. 2014, no. 1, pp. 1–14, 2014.
- [2] J. F. Euriques, C. P. Krueger, W. C. Machado, L. F. Sapucci, and F. Geremia-Nievinski, "Soil moisture estimation with gnss reflectometry: a conceptual review," *Revista brasileira de cartografia, Rio de Janeiro. Vol. 73, n. 2 (2021)*, p. 413-434, 2021.
- [3] ITU-R, *Electrical characteristics of the surface of the earth. Recommendation Rec. 527-6*, 2021.
- [4] W. H. Hayt Jr and J. A. Buck, *Eletromagnetismo*. Bookman Editora, 2013.
- [5] V. U. Zavorotny and A. G. Voronovich, "Bistatic gps signal reflections at various polarizations from rough land surface with moisture content," in *IGARSS 2000. IEEE 2000 International Geoscience and Remote Sensing Symposium. Taking the Pulse of the Planet: The Role of Remote Sensing in Managing the Environment. Proceedings (Cat. No. 00CH37120)*, vol. 7. IEEE, 2000, pp. 2852–2854.
- [6] V. de Paul Obade and R. Lal, "Towards a standard technique for soil quality assessment," *Geoderma*, vol. 265, pp. 96–102, 2016.
- [7] A. E. Egido, "Gnss reflectometry for land remote sensing applications," Ph.D. dissertation, Universitat Politècnica de Catalunya, 2014.
- [8] E. Motte, M. Zribi, P. Fanise, A. Egido, J. Darrozes, A. Al-Yaari, N. Baghdadi, F. Baup, S. Dayau, R. Fieuzal *et al.*, "Glori: A gnss-r dual polarization airborne instrument for land surface monitoring," *sensors*, vol. 16, no. 5, p. 732, 2016.
- [9] N. Rodriguez-Alvarez, A. Camps, M. Vall-Llossera, X. Bosch-Lluis, A. Monerris, I. Ramos-Perez, E. Valencia, J. F. Marchan-Hernandez, J. Martinez-Fernandez, G. Baroncini-Turricchia *et al.*, "Land geophysical parameters retrieval using the interference pattern gnss-r technique," *IEEE Transactions on Geoscience and Remote Sensing*, vol. 49, no. 1, pp. 71–84, 2010.
- [10] A. Alonso-Arroyo, A. Camps, A. Aguasca, G. Forte, A. Monerris, C. Ruediger, J. P. Walker, H. Park, D. Pascual, and R. Onrubia, "Improving the accuracy of soil moisture retrievals using the phase difference of the dual-polarization gnss-r interference patterns," *IEEE Geoscience and Remote Sensing Letters*, vol. 11, no. 12, pp. 2090–2094, 2014.
- [11] B. H. Fleury, M. Tschudin, R. Heddergott, D. Dahlhaus, and K. I. Pedersen, "Channel Parameter Estimation in Mobile Radio Environments Using the SAGE Algorithm," *IEEE Journal on Selected Areas in Communications*, vol. 17, no. 3, March 1999.
- [12] J. A. Fessler and A. O. Hero, "Space-Alternating Generalized Expectation-Maximization Algorithm," *IEEE Transactions on Signal Processing*, vol. 42, no. 10, October 1994.
- [13] B. M. Hannah, "Modelling and simulation of gps multipath propagation," Ph.D. dissertation, Queensland University of Technology, 2001.